



# 国立極地研究所

大学共同利用機関法人 情報・システム研究機構

Title	Polarization electric field inside auroral patches: Simultaneous experiment of EISCAT radars and KAIRA
Authors	Takahashi Toru, Virtanen Ilkka I., Hosokawa Keisuke, Ogawa Yasunobu, Aikio Anita, Miyaoka Hiroshi, Kero Antti
Citation	JGR : Space Physics, 124(5), 3543-3557, 2019
Issue Date	2019-4-1
Type	Journal Article
URL	<a href="https://doi.org/10.1029/2018JA026254">https://doi.org/10.1029/2018JA026254</a>
Right	
Textversion	publisher

## JGR Space Physics

## RESEARCH ARTICLE

10.1029/2018JA026254

## Key Points:

- The drift speed of auroral patches was consistent with the convective electric field
- The polarization electric fields perpendicular to the convective electric fields were generated inside the auroral patches
- The upward and downward FACs contacting the west and east side edges of the auroral patches weakened the polarization electric field

## Supporting Information:

- Supporting Information S1
- Movie S1

## Correspondence to:

T. Takahashi,  
takahashi.toru@nipr.ac.jp

## Citation:

Takahashi, T., Virtanen, I. I., Hosokawa, K., Ogawa, Y., Aikio, A., Miyaoka, H., & Kero, A. (2019). Polarization electric field inside auroral patches: Simultaneous experiment of EISCAT radars and KAIRA. *Journal of Geophysical Research: Space Physics*, 124, 3543–3557. <https://doi.org/10.1029/2018JA026254>

Received 3 NOV 2018

Accepted 26 MAR 2019

Accepted article online 1 APR 2019

Published online 8 MAY 2019

Corrected 10 JUN 2019

This article was corrected on 10 JUN 2019. See the end of the full text for details.

©2019. American Geophysical Union.  
All Rights Reserved.

## Polarization Electric Field Inside Auroral Patches: Simultaneous Experiment of EISCAT Radars and KAIRA

Toru Takahashi<sup>1</sup>, Ilkka I. Virtanen<sup>2</sup>, Keisuke Hosokawa<sup>3</sup>, Yasunobu Ogawa<sup>1,4</sup>, Anita Aikio<sup>2</sup>, Hiroshi Miyaoka<sup>1,4</sup>, and Antti Kero<sup>5</sup>

<sup>1</sup>National Institute of Polar Research, Tachikawa, Japan, <sup>2</sup>Ionospheric Physics Research Unit, University of Oulu, Oulu, Finland, <sup>3</sup>Department of Communication Engineering and Informatics, University of Electro-Communications, Chofu, Japan, <sup>4</sup>Department of Polar Science, SOKENDAI (The Graduate University for Advanced Studies), Tachikawa, Japan, <sup>5</sup>Sodankylä Geophysical Observatory, University of Oulu, Sodankylä, Finland

**Abstract** The primary focus of this study was the motion of auroral patches and the polarization electric field generated therein observed on 9 November 2015 in an experiment using the European incoherent scatter (EISCAT) radars, Kilpisjärvi Atmospheric Imaging Receiver Array (KAIRA), and an all-sky imager simultaneously. Based on the all-sky imager data, the drift speed of the auroral patches corresponded to a southward electric field of  $14.1 (\pm 3.7)$ – $17.2 (\pm 4.5)$  mV/m. The convective electric field derived from the EISCAT radars and KAIRA observation was approximately 14.6 mV/m in the southward direction. This suggests that the spatial distribution of the auroral patches reflects the distribution of the cold plasma in the magnetosphere. The electron density and the height-integrated Hall conductance between 80 and 120 km were enhanced by a factor of 2–4 inside the auroral patches. In this situation, a polarization electric field was generated therein. Enhanced ion velocities due to the polarization electric field was observed at up to 200-km altitude; however, the absolute values of the ion velocities were approximately 40% of what was expected from the polarization electric field. A field-aligned current (FAC) from 5 to 10  $\mu\text{A}/\text{m}^{-2}$  in the edges of the auroral patches could explain the weakening of the polarization electric field. Since a FAC of that order of magnitude corresponded with that observed by the Swarm satellite, it was suggested that the polarization electric field was weakened by the FAC. Furthermore, the polarization electric field propagated upward from the dynamo region to at least 200 km.

### 1. Introduction

The magnetic substorm onset is manifested by the expansion of the auroral oval and the brightness of the discrete aurora which shows a curtain-like structure. The discrete aurora is considered to be associated with the shear flow in the plasma sheet (Haerendel, 2007). At the recovery phase of the onset, the diffuse aurora typically appeared. In general, the diffuse aurora consists of a patch structure that often exhibits an optical pulsation. This pulsation is called pulsating auroras (PsA) that are known to be produced by quasiperiodic precipitations of highly energetic electrons with a period of a few seconds to a few tens of seconds (Miyoshi et al., 2015).

Polarization electric fields generated in both auroral arcs and auroral patches play an important role for the magnetosphere-ionosphere coupling, because the polarization electric field effect may change the current system including the ionospheric current and field-aligned current (FAC; Amm et al., 2013). In a previous study, de la Beaujardiere et al. (1977) conducted incoherent scatter radar observations at Chatanika, Alaska, and found the existence of the southward polarization electric field response to the ionospheric conductivity increasing inside auroral arcs. Since the high energetic particle precipitation can be typically seen as a diffuse aurora, many recent studies have focused on revealing the generation mechanisms and the intensity of the polarization electric field inside the auroral patch. For example, Hosokawa et al. (2008) observed a quasiperiodic oscillation in the line-of-sight (LOS) ion drift inside PsA patches using a SuperDARN radar and an all-sky imager in Iceland. That study showed that the ion drift oscillation was correlated with the optical pulsation of the PsA, appearing to be driven by polarization electric fields generated by charge separations at the edges of enhanced electron density regions due to PsA precipitation. To conduct a precise

evaluation of the polarization electric field generation by auroral precipitation, the European incoherent scatter (EISCAT) radars and an all-sky imager were simultaneously operated in Tromsø, Norway (Hosokawa et al., 2010). That experiment found that the polarization electric field (proportional to the Hall conductance enhancement) could be generated inside the PsA. The polarization electric field magnitude and direction were estimated using the electric current continuity between the inside and outside of the ionization region by the auroral precipitation as described in Marklund (1984) and Brekke (1997). Although the directions of the estimated and observed polarization electric fields were highly correlated with one another, the field strengths observed with radar were significantly lower than the estimates based on current continuity. To date, polarization electric field generation has not been quantitatively investigated because those previous studies did not measure the three-dimensional convective electric field.

Auroral patches typically tend to extend over hundreds of kilometers and are often observed in the morning sector during the substorm recovery phase (Akasofu et al., 1966). Auroral precipitation covers approximately 80-km altitude inside auroral patches and appears to generate a polarization electric field. Previous studies have focused on patch motion rather than the polarization electric field. Davis (1978) revealed that auroral patches moved with the ionospheric convection. Yang et al. (2015) extended this study using an all-sky imager and the SuperDARN radar and suggested that patch motion is governed by the  $\mathbf{E} \times \mathbf{B}$  drift and the patch source in the magnetosphere also moves with this drift. Those results indicate that shape and motion of the patches are related to the distribution of cold plasma in the magnetosphere, because motion of the cold plasma is governed by the  $\mathbf{E} \times \mathbf{B}$  drift. However, since the convective electric field estimation performed by the SuperDARN radar contains a large uncertainty, a precise measurement of patch motion has not yet been conducted.

The current study investigated the polarization electric field generated in the auroral patch through ion velocity observations in the F and E regions performed simultaneously by EISCAT radars and the Kilpisjärvi Atmospheric Imaging Receiver Array (KAIRA). Furthermore, this simultaneous experiment enabled an elaborate investigation of auroral patch motion to be conducted.

In section 2, we describe the instruments, the observational configuration, and the data sets. In section 3, the observational results are presented. In section 4, we derive the drift speed of the auroral patch and compare it with the convective electric field. In section 5, we compare the polarization electric field calculated by the enhancement of the Hall conductance with the vertical ion velocity. Moreover, the possible mechanism of the weakening of the polarization electric field is discussed. This paper ends with a summary in section 6.

## 2. Observation Setup

The EISCAT ultra high frequency (UHF) and very high frequency (VHF) radars have been installed at the facility in Ramfjordmoen, Tromsø, Norway (69.6° N, 19.2° E) with operating frequencies of 930 (UHF) and 244 MHz (VHF; Rishbeth & Williams, 1985). Remote antennas (radar receivers) have been also installed at Kiruna (67.9° N, 20.4° E) and Sodankylä (67.4° N, 26.6° E) to receive the backscatter echoes from the VHF radar pulses.

Between 18:00 UT on 8 November 2015 and 6:00 UT on 9 November 2015, the auroral activity was high. The solar wind speed varied from 426.1 to 563.4 m/s, and the interplanetary magnetic field ( $B_z$ ) was almost negative. The  $B_z$  temporally became positive around 19:30, 21:30, 1:00, and 2:00 UT, but the magnitude was mostly less than 1 nT.

The 3 hr Kp indices were 4+, 4, 4, and 4-. The EISCAT UHF and VHF radars operated from 00:00 to 04:00 UT on 9 November 2015 and provided ion velocities and electron densities in the LOS direction with a temporal resolution of 1 min. The EISCAT UHF radar was pointed eastward at the elevation angle of 75°. The VHF beam was pointed vertically and was used in a tristatic mode with the Kiruna and Sodankylä remote antennas. VHF beam intersections of the Kiruna and Sodankylä radar remote antennas were set to an altitude of 320 km at the topside of the F region from 02:19 to 03:24 UT. From 00:00 to 02:18 and 03:35 to 04:00 UT, this intersection was set to 240 km. A tristatic radar consisting of the VHF, Kiruna, and Sodankylä radars provided three-dimensional ion velocities and the electric field at the intersection altitude.

During this experiment, the EISCAT UHF and VHF radars were operated with the “beata” pulse code. The beata pulse code is designed for both the E and F region observations and has been used for common programs of the EISCAT UHF and VHF radars. The beata uses one 32-bit alternating code with baud length of

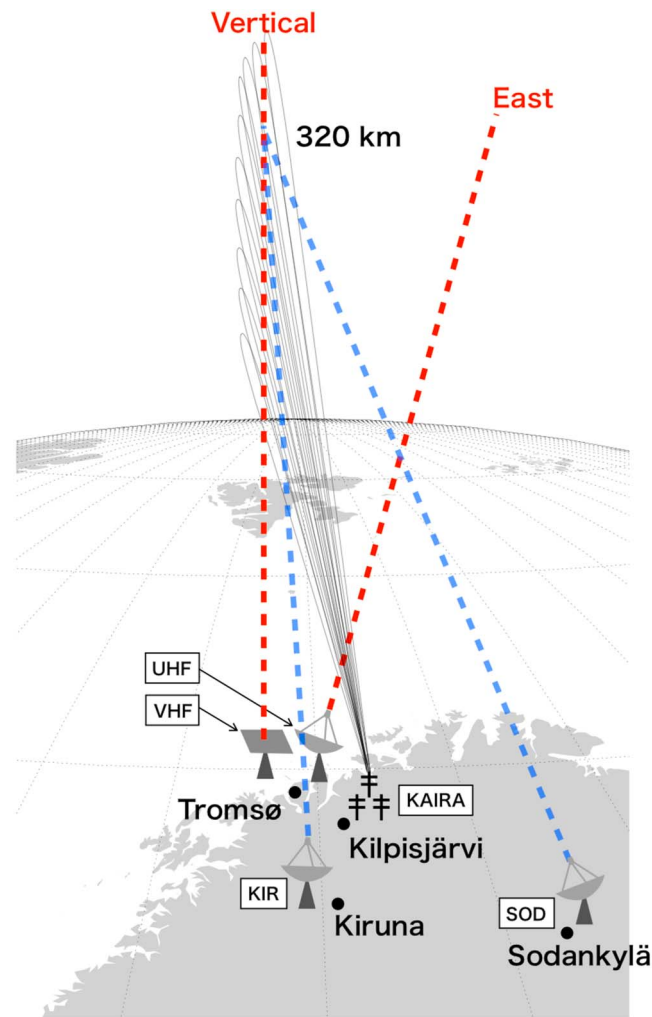


**Figure 1.** Observation configuration of EISCAT UHF, VHF, Kiruna (KIR), Sodankylä (SOD) radars, and KAIRA on 9 November 2015 from 02:30 to 03:20 UT. Red dashed lines show the transmission radar beam and backscatter echo path. Blue dashed lines show only backscatter echo path. The KAIRA received backscatter echoes from the VHF radar pulses with 10 beams as shown by the black thin fan-like shape.

$20 \mu\text{s}$ . Sampling rate and range coverage of the beata for UHF (VHF) radar are  $10 \mu\text{s}$  ( $20 \mu\text{s}$ ) and 49–693 km (52–663 km), respectively.

The KAIRA installed in Kilpisjärvi, Finland ( $69.1^\circ \text{ N}$ ,  $20.8^\circ \text{ E}$ ), was operated simultaneously with the EISCAT radars from 00:00 to 04:00 UT and received backscatter echoes from the VHF radar pulses with 10 beams that covered the F region part of the ionosphere. In this study, we tried to suppress the electric field variance by adopting a new calculation method for incoherent scatter spectra from EISCAT radars and KAIRA which described below. In conventional incoherent scatter analysis, plasma parameters are fitted to incoherent scatter spectra from each radar site separately, and the velocity is estimated from the LOS velocity estimates in an additional analysis step. In the multistatic analysis (Virtanen et al., 2014), spectra from all sites are collected together, and both scalar (electron density and electron and ion temperature) and vector (ion velocity and possibly ion temperature anisotropy) parameters are fitted in a single analysis step. The multistatic analysis improves statistical accuracy of both scalar and vector parameters, because the information contained in the remote receiver data is optimally used. In this case, observations along up to five different LOS directions were combined. For this observation, using KAIRA observations in addition to the tristatic and UHF radar observations, electric field variances could be suppressed by 40–80%. This combination enables us to derive the ionospheric electric field with sufficient accuracy to evaluate the polarization electric field. The three-dimensional electric field was calculated with a temporal resolution of 1 min using

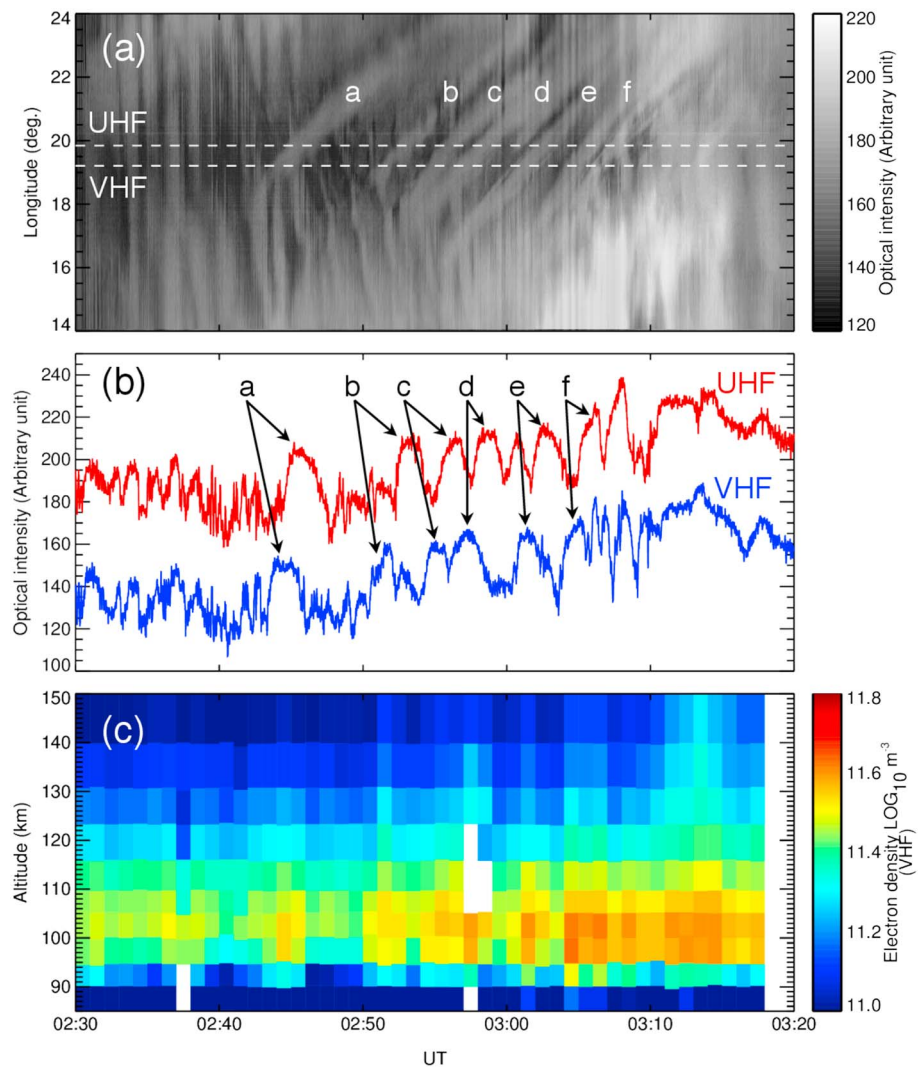


**Figure 2.** (a) Keogram in the east-west cross section from the all-sky Watec imager, (b) the time series of the emission intensity at the UHF (red) and VHF (blue) beam position, and (c) the electron density observed by the EISCAT VHF radar with a 1-min temporal resolution for the time interval 02:30 to 03:20 UT on 9 November 2015. The EISCAT UHF and VHF beam position in the keogram was shown by white dashed lines in the (a). The emission intensity at the UHF radar beam position was added 50.

ion velocities from 200 to 400 km observed by the EISCAT UHF, VHF, Kiruna, Sodankylä radars, and KAIRA (McKay-Bukowski et al., 2015). The details of the calculation method are described in Virtanen et al. (2014).

In addition, auroral images were captured by an all-sky Watec imager (AWI) at Tromsø operated by the National Institute of Polar Research, Japan. A broadband optical filter ( $\sim 500\text{--}600$  nm) covering the auroral 557.7-nm emission was mounted on the AWI system, and the green line all-sky images were obtained every 1 s. The observation configuration is illustrated in Figure 1.

Here we applied the following methods to evaluate the polarization electric field generated in the E region. The north-southward component of the polarization electric field accelerates ion in the east-west direction. As shown in Figure 1, the UHF radar that was pointed eastward with a  $75^\circ$  elevation angle can observe this ion acceleration. However, the east-westward polarization electric field caused both the horizontal northward and vertical ion drifts to accelerate because the magnetic field of the earth has an inclination of approximately  $78^\circ$  at Tromsø. Vertical ion drift was almost equal to the 20% of the ion drift caused by the polarization electric field. An eastward polarization electric field of approximately 30 mV/m, which is an expected intensity of the polarization electric field, would result in maximum vertical ion velocities of  $\sim 100$  m/s. Because this velocity is greater than the typical measurement error of the ion velocity around

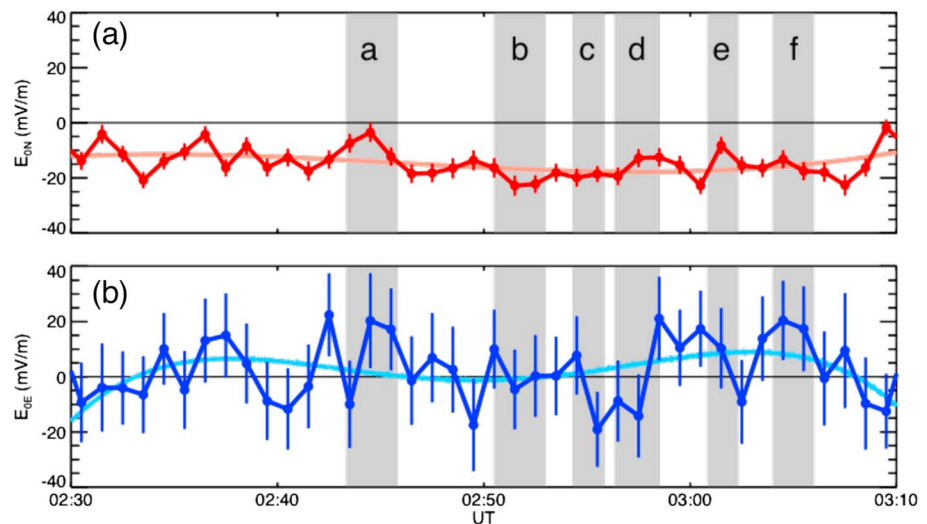


**Figure 3.** The (a) northward electric field ( $E_{0N}$ ) and the (b) eastward electric field ( $E_{0E}$ ). The electric field component was derived by the EISCAT UHF, VHF, Sodankylä, Kiruna radars, and KAIRA experiment. Gray shades show the time interval when the EISCAT VHF radar detected auroral patches. The light blue and red lines were derived from the four-degree polynomial fit applied to the eastward and northward electric field to obtain  $E_0$  in section 5.

100 km observed by the VHF radar, the influence of the polarization electric field on the observed ion velocity was evaluated via the VHF radar data.

### 3. Observation Results

Figure 2a shows a keogram of the AWI data along the east-west cross section. It can be seen from Figure 2a that a vertical stripe pattern (indicative of PsA) was present in the keogram throughout the entire interval. After 02:40 UT, six oblique traces were captured traversing the keogram from the upper right to lower left. They are also seen as emission intensity peaks at the UHF and VHF beam positions shown in Figure 2b. These peaks indicate that patch structures traveled eastward. There was no optical pulsation in the auroral patch in the AWI data with a 1-s temporal resolution. Thus, in this paper, the patch structures are called auroral patch and labeled sequentially as a–f as they pass through the fields of view (FOVs) of the UHF and VHF radars.

The electron density observed at 80–150-km altitude by the VHF radar is shown in Figure 2c. It can be seen that the electron density between 90 and 100 km was approximately  $10^{11.5} \text{ m}^{-3}$  from 02:30 to 02:40 UT, before the passage of the auroral patches. This high electron density was likely the result of precipitation associated with the PsA or background activity. Subsequently, the electron density was enhanced to  $10^{11.6}$ – $10^{11.7} \text{ m}^{-3}$  when the auroral patches passed across the FOV of the VHF radar. Thus, the ionization due to auroral precipitation inside the auroral patches was stronger than the PsA ionization.

### 4. Motion of Auroral Patches

The cross correlation was calculated as a function of time difference  $\tau$  between  $I_{\text{UHF}}(t)$  and  $I_{\text{VHF}}(t)$ , which are the emission intensities at the UHF and VHF beam positions shown in Figure 2b, respectively. According to this analysis, the auroral patch detection time difference between the UHF and VHF beam positions was 77 s. Here we define the correlation coefficient greater than 0.75 as a criterion for high correlation. Since the correlation coefficient is over 0.75 within  $\tau = 77 \pm 20$  s, the estimation error of the auroral patch detection time difference ( $\sigma_\tau$ ) was assumed to be 20 s. In the following paragraph, we derive the drift speed of the auroral patch from this drift time ( $77 \pm 20$  s) and the distance between the UHF and VHF radar beam positions.

The height of the auroral emission layer must be estimated first to calculate the auroral patch drift speed because the distance between the FOVs of the UHF and VHF radars gradually separate with increasing altitude as shown in Figure 1. As is shown later in Figure 4a, ionization by auroral precipitation primarily occurred between altitudes of 80 and 120 km, with a peak altitude of 97 km. Thus, the emission layer was

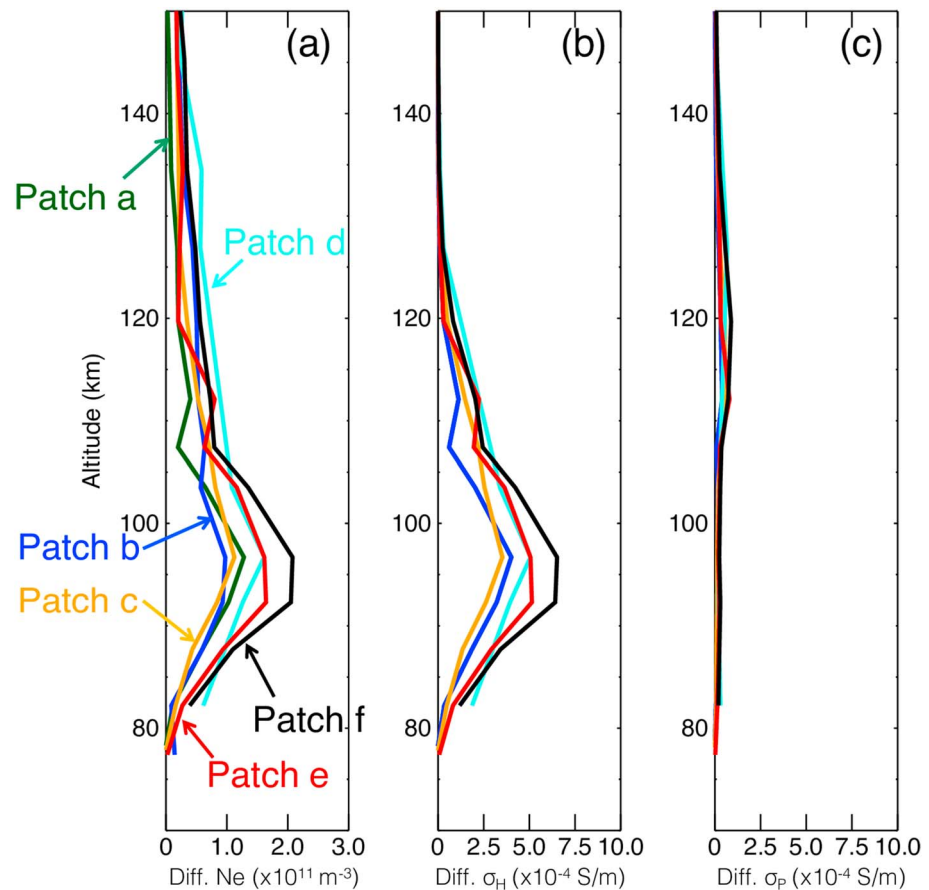


**Figure 4.** Vertical profile of the deviation from (a) the background of the electron density (Ne), (b) the Hall conductance, and (c) the Pedersen conductance inside the auroral patches. Profiles for the patches “a–f” were obtained at 02:44:30, 02:51:30, 02:55:30, 02:57:30, 03:01:30, and 03:04:30 UT, respectively.

assumed to be located within the height range of 90–110 km. At 90 and 100 km, the distances between the FOVs are approximately 24.1 and 29.5 km. Moreover, the beam broadening is also important to estimate the distance uncertainty, because the time series of the optical intensity shown in Figure 2b was assumed to be observed in the VHF and UHF radar beam. The beam width of the VHF and UHF radars is defined by the full width at half maximum of the transmitted wave power ( $\sim 2\sigma$ ), and the beam shape is similar to a Gaussian profile. The UHF and VHF radar beam widths are  $0.7^\circ$  and  $1.4^\circ$ , respectively. The UHF (VHF) radar beam width is 1.1 (2.2) km at 90 km and 1.3 (2.7) km at 110 km. Thus, the uncertainty in distance is estimated to 1.2 km at 90 km and to 1.5 km at 110 km.

Based on above analysis and assumption, the auroral patch passed the distance from  $24.1(\pm 1.2)$  to  $29.5(\pm 1.5)$  km in  $77(\pm 20)$  s. If the emission layer is assumed to have been located from 90 to 110 km, drift speeds of the auroral patches would have ranged from approximately  $313(\pm 83)$  to  $383(\pm 101)$  m/s. Assuming  $4.5 \times 10^{-5}$  T (International Geomagnetic Reference Field) (Thébault et al., 2015) for the background magnetic field near the radar sensing area, the magnitude of the corresponding electric field at 90 and 110 km would be  $14.1(\pm 3.7)$  and  $17.2(\pm 4.5)$  mV/m, respectively.

Figures 3b and 3c show the northward and eastward electric field perpendicular to the magnetic field calculated by the ion velocities from 200 to 400 km obtained by combining data from the EISCAT UHF, VHF, Kiruna and Sodankylä radars, and KAIRA (Virtanen et al., 2014). The northward electric field could be derived more accurately than the eastward electric field, because the UHF radar was pointed eastward during the experiment. The mean values of the northward and eastward electric fields from 02:30 to 03:10 UT were  $-14.6$  and  $2.28$  mV/m, respectively. This electric field was considered to be the background convective electric field in the ionosphere. The northward electric field observed by the EISCAT radars and KAIRA was within the range of the electric field estimated by the eastward drift speed of the auroral patches.

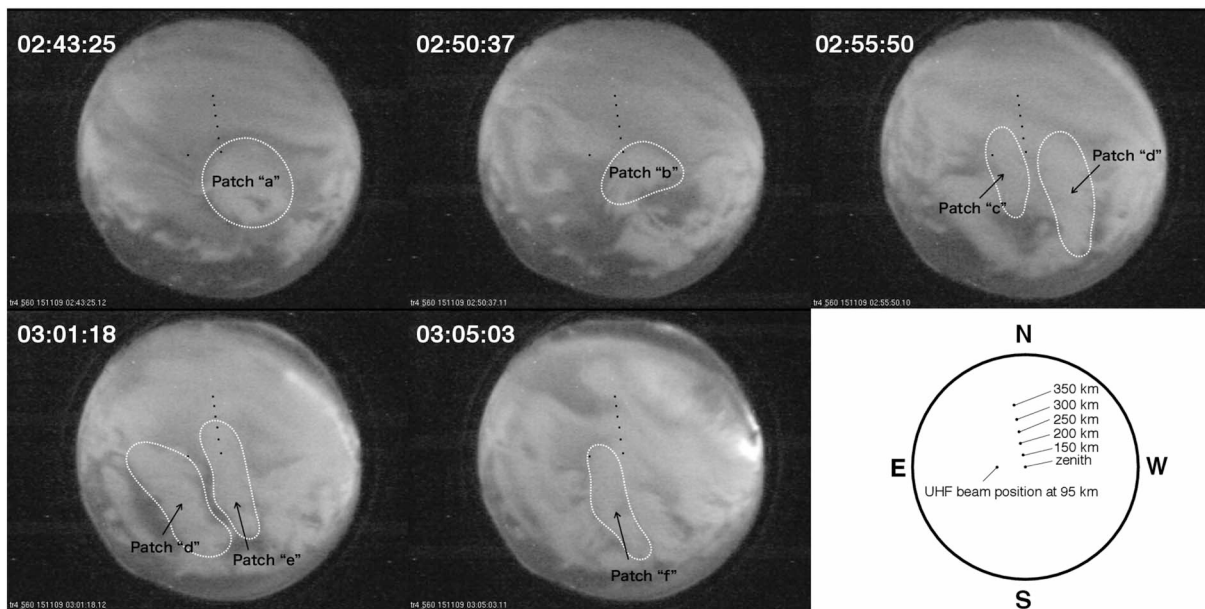


**Figure 5.** All-sky images at 02:43:25, 02:50:37, 02:55:50, 03:01:18, and 03:05:03 UT and footprints from 150, 200, 250, 300, and 350 km to 95 km at zenith of Tromsø.

( $14.1 \pm 3.7$ – $17.2 \pm 4.5$  mV/m). This agreement is likely to indicate that the motion of the auroral patches follows the convective electric field. The motion of the hot plasma in the magnetosphere follows trajectories of the gradient B and curvature drift. On the other hand, the motion of cold plasma in the magnetosphere is governed by the  $\mathbf{E} \times \mathbf{B}$  drift (Oguti, 1976). Therefore, the connection between the patch motion and the convective electric field suggests that the spatial distribution of auroral patches reflects the distribution of cold plasma in the magnetosphere.

## 5. Polarization Electric Field

In this section, the polarization electric field generated inside the auroral patches will be evaluated and discussed. At first, in section 5.1, by deriving the Hall and Pedersen conductance inside and outside the auroral patches, we evaluated whether the polarization electric field was generated or not. We then described its evaluation method in the section 5.2. In sections 5.3 and 5.4, the polarization electric field will be estimated based on the charge separation mechanisms due to the current continuity, and the enhanced ion velocities associated with the estimated polarization electric field will be compared with the ion velocity observed by the VHF radar. As will be explained at the end of this section, to discuss the cause of the weakening of the polarization electric field, we consider the contribution of the field-aligned current (FAC) to the cancelation or weakening of the charge separation.

### 5.1. Hall Conductance Enhancement Inside Auroral Patches

The VHF radar observed outside the auroral patch from 02:47:30 to 02:48:30 UT. Thus, the background was defined by the mean profiles obtained at that time. Figures 4a–4c show electron density and the Hall and Pedersen conductances, respectively, as deviations from their background values inside the auroral patches a–f as identified in Figure 2. It can be seen in Figures 4a and 4b that the electron densities and Hall conductances inside the auroral patches were enhanced in the range of 80–120 km with a peak altitude of approximately 97 km. The Pedersen conductance enhancement, conversely, was negligibly small relative to the Hall conductance enhancement as can be seen in Figure 4c. Hosokawa et al. (2010) indicated that the polarization electric field can be generated inside the PsA patch when the Hall conductance is enhanced in the PsA patch and the Pedersen conductance is uniform. Since the situation inside and outside of the auroral patches a–f is almost the same as their study, the polarization electric field is assumed to be generated in the dynamo region, between 80- and 120-km altitude.

The westward Hall current increased in the auroral patches because of the Hall conductance enhancement. In this situation, the east (west) edge of the auroral patches becomes negatively (positively) charged to main-

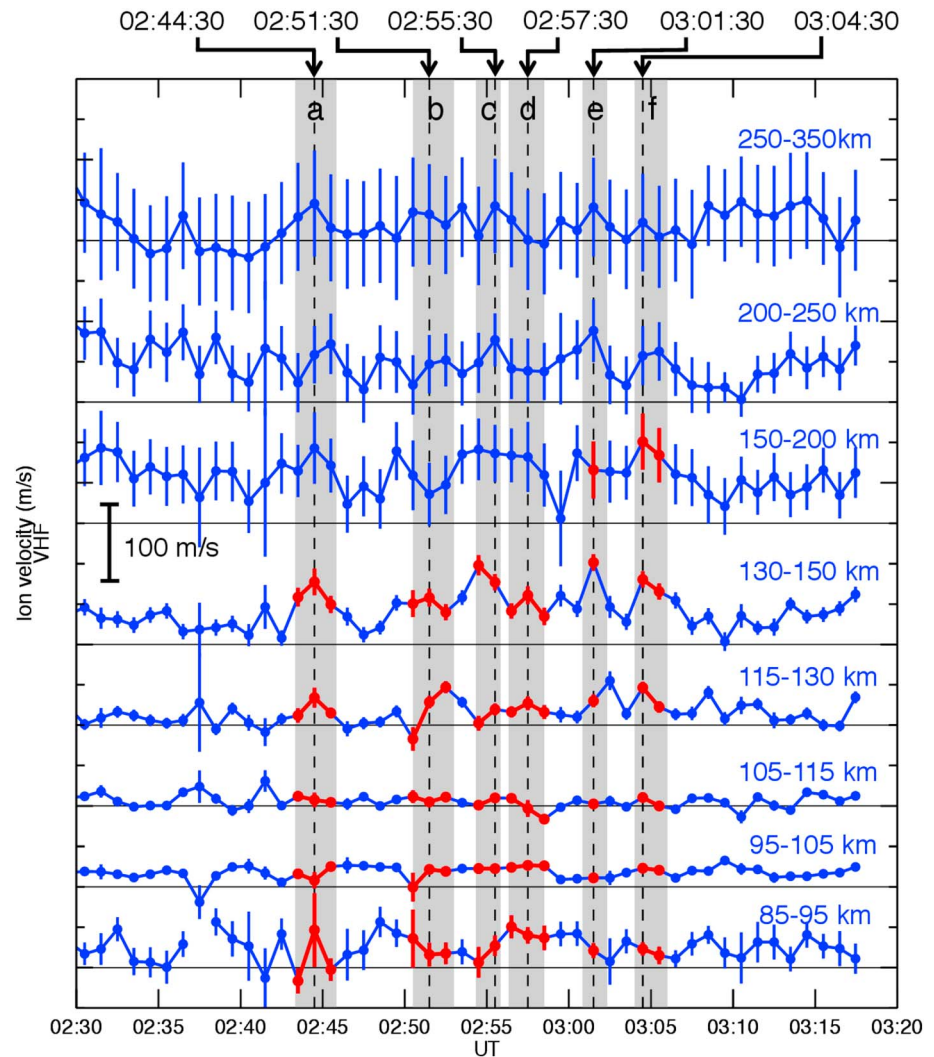


**Figure 6.** Vertical ion velocity observed by the VHF radar. Upward is positive. Red dots and lines indicate when the ion velocity was possibly influenced the polarization electric field generated inside the auroral patches. Gray shades show the time interval when the auroral patches were detected by the VHF radar.

tain the current continuously. From this charge separation, the direction of the polarization electric field was estimated to be approximately eastward. Furthermore, if the component of the northward polarization electric field was large, the eastward ion drift would be accelerated. However, the UHF radar, which was pointed to east, detected no remarkable enhancements of the east-westward ion velocity inside the auroral patch. This observational result of the UHF radar also supports that polarization electric field direction was approximately eastward. Since the eastward polarization electric field accelerated the geographically northward and vertical ion drift, the vertical ion drift observed by the VHF radar was used to evaluate the polarization electric field.

As mentioned in Hosokawa et al. (2010), the PsA that simultaneously appeared with the auroral patches probably generated the polarization electric field. However, the emission region of the PsA elongated more in the east-west direction (not a patch structure). We were not able to identify the eastern and western edges of the emission region from the AWI data. The charge separation, which is the cause of the polarization electric field, was hardly introduced at the eastern and western edges during our experiment. Since the PsA observed on 9 November 2015 did not have patch structure similar to the one presented in Hosokawa et al. (2010), we assumed that the PsA did not generate the polarization electric in this current interval.

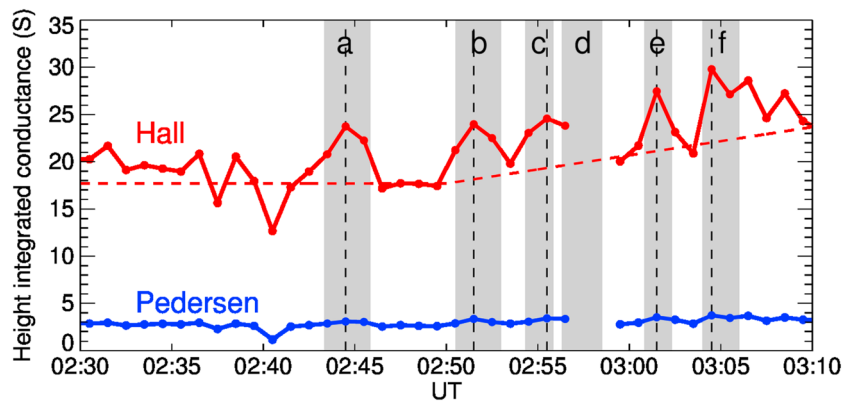


**Figure 7.** Height-integrated Hall and Pedersen conductances from 80 to 120 km with 1-min temporal resolution. The red dashed line shows the background Hall conductance.

### 5.2. Evaluation Method for the Polarization Electric Field

The polarization electric field propagates along the magnetic field (Mozer, 1970). Because the VHF radar observes the ion velocity at several altitudes along the vertical radar beam, the VHF observations can also be used for studying the upward propagation of the polarization electric field along the magnetic field. However, this is only possible if the magnetic footprint of the observed plasma volume is within the auroral patch. The field propagation can be observed up to the altitude at which the footprint at the patch height reaches the patch edge. For example, the magnetic field at 300-km altitude directly above the radar site is connected to a point approximately 44-km north of the site at an altitude of 95 km.

Figure 5 and Movie S1 of the supporting information show the all-sky images and field footprints captured at different altitudes of 150, 200, 250, 300, and 350 km at the Tromsø zenith. The 200-km footprint was located north of auroral patches “a,” “b,” “c,” and “d” but was located inside patches “e” and “f.” This positional relationship between the footprints and auroral patches indicates that the VHF radar could detect upward propagation of the polarization electric field by evaluating the ion velocity up to 150 km in auroral patches “a,” “b,” “c,” and “d” and up to 200 km in the auroral patches “e” and “f.”

The EISCAT radar can provide the ion velocity at altitudes of 88, 92, 97, 103, 107, 112, 120, 127, 134, 145, 156, 166, 180, and 193 km. The ion velocities were averaged across several altitude layers such as 85–95, 95–105, 105–115, 115–130, 130–150, and 150–200 km. Figure 6 shows the averaged vertical ion velocity observed by the VHF radar. Red dots and lines indicate the ion velocity, possibly influenced by the polarization electric field generated inside the auroral patches based on the AWI data, as described in the above paragraph. Gray shades indicate the time intervals when the auroral patches passed through the FOV of the VHF radar. The time intervals for the auroral patches from “a” to “f” were 2:43:20–2:45:50, 2:50:30–2:53:00, 2:54:20–2:55:50, 2:56:20–2:58:30, 3:00:50–3:02:20, and 3:03:00–3:06:00 UT, respectively. Above 115 km, the ion velocities tended to increase during the passage of auroral patches; however, below 115 km, no clear velocity enhancements could be seen within the auroral patches. This characteristic appears to reflect the ion acceleration caused by the polarization electric field, which was generated inside the auroral patches. The ions below 115 km were also accelerated by the polarization electric field, but the acceleration was very small because the collision frequency between ions and neutral particles is substantially smaller than the ion gyro frequency. The ion velocity enhancements are discussed later in a more quantitative fashion.

### 5.3. Estimation of the Polarization Electric Field

Figure 7 shows a time series of the height-integrated Hall and Pedersen conductances from 80 to 120 km with a 1 min temporal resolution. The neutral atmospheric composition and the magnetic field of the earth were given by the NRLMSISE-00 empirical model (Bilitza, 2001; Picone et al., 2002) and the International Geomagnetic Reference Field model, respectively. During the time when auroral patch “d” was observed, a large measurement error in the electron density occurred, this measurement was therefore excluded from the conductance calculations. As shown in Figure 4c, the Pedersen conductance varied slightly, with a mean value of 2.74 S and a standard deviation of 0.45 S between 02:30 and 03:10 UT. Thus, the Pedersen conductance was assumed to be unaffected by the auroral precipitation.

**Table 1**

*The Height-Integrated Pedersen Conductance ( $\sigma_P$ ), the Enhancement of the Hall Conductance ( $\Delta\sigma_H$ ) from 80 to 120 km, and Their Ratio ( $\Delta\sigma_H/\sigma_P$ )*

Patch	$\sigma_P$ (S)	$\Delta\sigma_H$ (S)	$\Delta\sigma_H/\sigma_P$
a	3.06	6.07	1.98
b	3.34	6.15	1.84
c	3.40	5.60	1.65
d	—	—	—
e	3.51	6.55	1.87
f	3.71	7.91	2.13

To calculate the magnitude of the polarization electric field, the background Hall conductance level was defined. The background Hall conductance from 02:30 to 02:50 UT was evaluated to 17.7 S by averaging the Hall conductance from 02:47:30 to 02:48:30 UT. From Figures 2b and 2c, it can be seen that both the emission intensity and the electron density increased simultaneously after 02:50 UT due to PsA precipitation. This coincidence indicates that the PsA increased the electron density and Hall conductance backgrounds. Thus, the background Hall conductance was assumed to be gradually increasing with  $5 \times 10^{-3}$  S/s after 02:50 UT. The intersection points between the black and red dashed lines illustrated in Figure 7 indicate the background Hall conductance for each auroral patch. The deviations of the Hall conductance from the background ( $\Delta\sigma_H$ ), the Pedersen conductance ( $\sigma_P$ ), and the ratio of  $\Delta\sigma_H$  to  $\sigma_P$  are summarized in Table 1.

The polarization electric field was calculated from the Hall conductance enhancement ( $\Delta\sigma_H$ ) and the convective electric field ( $E_0$ ). First, the auroral patch spatial structures were assumed to be elongated in the north-south direction, and the divergence of the electric current was assumed to be zero in the ionosphere ( $\nabla \cdot \mathbf{J} = 0$ ). Therefore, the polarization electric field was calculated from the current continuity perpendicular to the convective electric field because the direction of the convective electric field was approximately southward. The current continuity perpendicular to the convective electric field is expressed as follows:

$$(\sigma_H + \Delta\sigma_H)E_0 - \sigma_P E_P = \sigma_H E_0, \quad (1)$$

where  $\sigma_H$  is the Hall conductance and  $E_P$  is the polarization electric field. Equation (1) ignores the FAC for its setup, and its left and right sides indicate the electric currents perpendicular to the convective electric field inside and outside the auroral patch, respectively. Solving equation (1) for  $E_P$  gives the following equation:

$$E_P = \frac{\Delta\sigma_H}{\sigma_P} E_0. \quad (2)$$

$\Delta\sigma_H/\sigma_P$  was already derived above and is listed in Table 1, and  $E_0$  can be derived from  $E_0 = \sqrt{E_{0E}^2 + E_{0N}^2}$ .  $E_{0E}$  and  $E_{0N}$  were the eastward and northward components of  $E_0$  and observed by the EISCAT radars and KAIRA are shown as thick blue and red lines with error bars in Figures 3a and 3b. The error bars indicate the statistical 1- $\sigma$  error estimates. The light blue and red lines in Figures 3a and 3b were derived from

**Table 2**

*The Magnitude of the Convective and Polarization Electric Field*

Patch	$E_{0E}$ (mV/m)	$E_{0N}$ (mV/m)	$E_0$ (mV/m)	$\theta$ ( $^\circ$ )	$E_P$ (mV/m)	$E_{PE}$ (mV/m)	$E_{PN}$ (mV/m)
a	1.40	-14.0	14.1	174	27.9	27.8	2.77
b	-0.71	-16.7	16.8	182	30.8	30.8	-1.30
c	1.86	-17.5	17.6	174	29.0	28.9	3.06
d	4.50	-17.7	18.3	166	—	—	—
e	8.55	-17.2	19.2	154	35.8	32.0	16.0
f	7.59	-15.5	17.2	154	36.8	33.0	16.2

*Note.*  $E_{0E}$  and  $E_{0N}$  are the eastward and northward component of the convective electric field.  $E_{PE}$  and  $E_{PN}$  are the eastward and northward components of the polarization electric field.  $\theta$  is the azimuth angle of  $E_0$  from north in the clockwise direction.

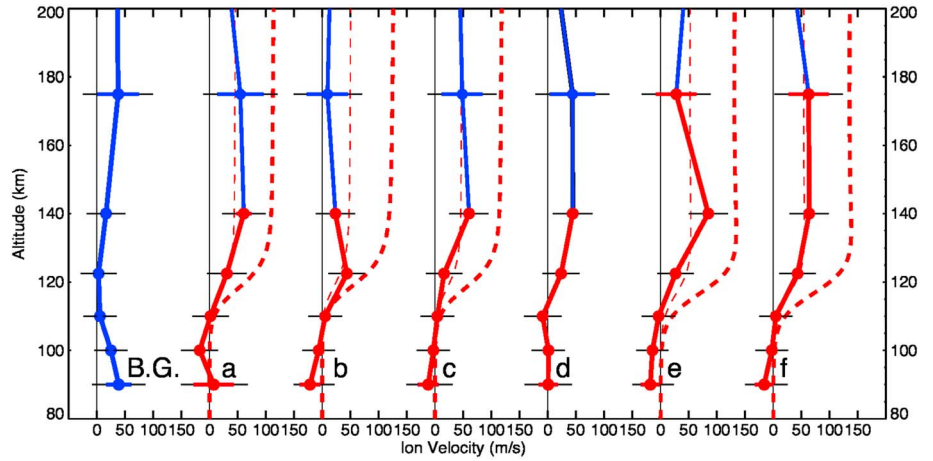


**Figure 8.** Height profile of  $v_{iP}$  for each auroral patch observed by the VHF radar. Red dots show the ion velocity influenced by the auroral patches. The leftmost line is defined as the background ion velocity averaged from 02:47:30 to 02:48:30 UT. The blue and red bars show the measurement error. The black bar shows the fluctuation related to the neutral wind. The red thick and thin dashed line is the estimated ion velocity for  $E_P$  and the 40% weakened  $E_P$ .

the four-degree polynomial fit without weighting applied to  $E_{0E}$  and  $E_{0N}$  from 02:30 to 03:10 UT.  $E_{0N}$  was relatively stable, whereas  $E_{0E}$  varied in the range of  $2\text{-}\sigma$  ( $\sim 30$  mV/m) from 02:30 to 03:10 UT.

$E_0$ ,  $E_{0E}$ ,  $E_{0N}$ , and  $E_P$  calculated with equation (2) are summarized in Table 2.  $E_{PE}$  and  $E_{PN}$  are the eastward and northward polarization electric field. According to those values,  $E_P$  was approximately twice as strong as  $E_0$  with a near-east direction. As mentioned above, since the magnetic field of the Earth has an inclination of approximately  $78^\circ$  at Tromsø, the eastward electric field causes both horizontal northward and vertical ion drifts. This enables the VHF radar to detect the vertical ion drift associated with  $E_{PE}$ . However,  $E_{PN}$  also caused the eastward ion drift enhancement with a maximum absolute value of several meters per second, which made it difficult to observe the ion velocity driven by  $E_{PN}$  with the UHF radar.

#### 5.4. Comparison of the Estimated Polarization Electric Field With Observed Ion Velocities

The vertical ion velocity  $v_i$  was divided into a background component  $v_{i0}$  and a secondary component  $v_{iP}$  influenced by  $E_P$ .

$$v_i = v_{i0} + v_{iP}. \quad (3)$$

$v_{i0}$  driven by  $E_0$ , the neutral wind, and diffusion.  $v_{iP}$  and  $v_{i0}$  can be derived from the equations of motion for ions as follows:

$$v_{iP} = \frac{\Omega_i^2}{v_{in}^2 + \Omega_i^2} \frac{E_{PE}}{B} \cos I + \frac{v_{in}\Omega_i}{v_{in}^2 + \Omega_i^2} \frac{E_{PN}}{B} \cos I \quad (4)$$

$$v_{i0} = \frac{\Omega_i^2}{v_{in}^2 + \Omega_i^2} \left( \frac{E_{0E}}{B} - W_N \sin I \right) \cos I + \frac{v_{in}\Omega_i}{v_{in}^2 + \Omega_i^2} \left( \frac{E_{0N}}{B} + W_E \right) \cos I + \left( 1 - \frac{\Omega_i^2 \cos^2 I}{v_{in}^2 + \Omega_i^2} \right) W_V + \alpha, \quad (5)$$

where  $I$  is the inclination of the magnetic field;  $v_{in}$  is the ion-neutral collision frequency;  $\Omega_i$  is the ion gyro-frequency;  $W_N$ ,  $W_E$ , and  $W_V$  are the geographically northward, eastward, and vertical (positive upward) neutral wind velocities, respectively; and  $\alpha$  is a term containing other contributing factors such as, for example,

**Table 3**  
The Range of the Horizontal Eastward ( $W_E$ ), Northward ( $W_N$ ), and Vertical ( $W_V$ ) Neutral Wind Velocities Substituted to Equation (5)

	Neutral wind velocity (m/s)
$W_E$	$\pm 150$
$W_N$	$\pm 150$
$W_V$	$\pm 20$

diffusion.  $v_{i0}$  was separated from  $v_i$  to evaluate the magnitude of the polarization electric field. We estimated the background ion velocity profile  $v_{i0}$  from the VHF data for the interval 02:47:30–02:48:30 UT in between where the patches “a” and “b” passed over the VHF beam location.

The fluctuation of  $E_{0E}$  was ignored by using the four-degree polynomial fit, but we discuss the influence of the fluctuation of  $E_{0E}$  on the estimation and evaluation of  $E_p$  below. When  $E_{0E}$  fluctuated in the range of 15 mV/m ( $\sim 1\text{-}\sigma$ ) from the light blue line shown in Figure 3b,  $E_{PN}$  also fluctuated in the range of approximately 30 mV/m. As described above,

$E_p$  was evaluated by conversion to the vertical ion velocity using equation (4) and comparison with the ion velocity observed by the VHF radar. The second term of equation (4) includes  $E_{PN}$ . However, the second term is substantially smaller than the first term of equation (4) that includes  $E_{PE}$  above 100 km. Thus, if  $E_{0N}$  is accurately derived, the influence of  $E_{0E}$  fluctuations on the evaluation of  $E_p$  is small.

Figure 8 shows the  $v_{iP}$  height profile inside the auroral patches observed by the VHF radar. Red dots show  $v_{iP}$ , and the leftmost profile labeled “B.G.” shows  $v_{i0}$ .  $v_{iP}$  was calculated by subtracting  $v_{i0}$  (given by equation (5)) from the ion velocity data for each patch (obtained at 02:44:30, 02:51:30, 02:55:30, 02:57:30, 03:01:30, and 03:04:30 UT) shown as red dots in Figure 6. Figure 8 shows that almost all ion velocities were upward and tended to increase at higher altitudes. These characteristics could be observed up to 200-km altitude. This result suggests that a polarization electric field existed inside each auroral patches and propagated up to at least 200 km.

The thick dashed line in Figure 8, representing the expected ion velocity, was calculated from equation (4) using  $E_p$  values as listed in Table 2. The maximum differences across all patches between the observed and expected ion velocity of each patch were 25, 85, 96, and 103 m/s and are located at 110, 122, 140, and 175 km, respectively. Since these differences could not be explained by the VHF radar measurement error as shown by the error bars in Figure 8 that indicate errors in fitting incoherent scatter spectra (Vallinkoski, 1988), we investigated a possible cause of this difference. As described above, the averaged ion velocity from 02:47:30 to 02:48:30 UT was defined as  $v_{i0}$ , assuming that  $v_{i0}$  was temporally constant.

However, the horizontal and vertical neutral winds typically changed within a range of  $\pm 150$  and  $\pm 20$  m/s according to Ishii et al. (1999) and Kurihara et al. (2009; listed in Table 3). If  $W_N = -150$  m/s,  $W_E = 150$  m/s and  $W_V = 20$  m/s,  $v_{i0}$  increased by about 50 m/s. Although such case is rare,  $v_{i0}$  fluctuations are shown in Figure 8 as the black error bar. These fluctuations related to the neutral wind are smaller than the differences between the observed and expected results. Therefore,  $E_p$  as calculated by equation (2) seems to be weakened by a mechanism that will be further investigated below.

To evaluate the weakening of the polarization electric field,  $E_p$  was gradually decreased in 10% steps (90%, 80%, 70%, ..., 10%) from the absolute value of  $E_p$ . After that the enhanced ion velocities were calculated for each weakened  $E_p$ . This evaluation method facilitates a comparison with previous studies. As a result of this, we found that the difference between the observed and calculated  $v_{iP}$  would be minimized by a 40% weakening of  $E_p$ . Hosokawa et al. (2010) showed that 70% of the charge separation was eliminated in the PsA patch, meaning that the polarization electric field was weakened to 30%, which is comparable to our results. The cause, which weakens polarization electric fields to approximately 30–40% of their initial strength, seems to be a general feature of auroral patches.

Next we investigate to check whether  $E_{PE}$  can be seen in the eastward electric field observed by the EISCAT radars and KAIRA experiment as shown in the Figure 3b. If the auroral patch included both the FOV of the UHF and VHF radars, we can derive the electric field inside the auroral patch. According to the time series of the emission intensity shown in Figure 2b, the UHF and VHF radars simultaneously detected the auroral patches “a,” “e,” and “f.” When these auroral patches passed through the zenith of Tromsø, the eastward electric fields for the auroral patches “a,” “e,” and “f” were 20.3, 10.3, and 20.4 mV/m, respectively. The calculated  $E_{PE}$  are 11.1, 12.8, and 13.2 mV/m with the assumption that the polarization electric field was weakened to 40% (refer to the paragraph above). Since the  $1\text{-}\sigma$  of the electric field observation was about 15 mV/m, the calculated  $E_{PE}$  was within the range of the error bar. Therefore, the EISCAT radars and KAIRA

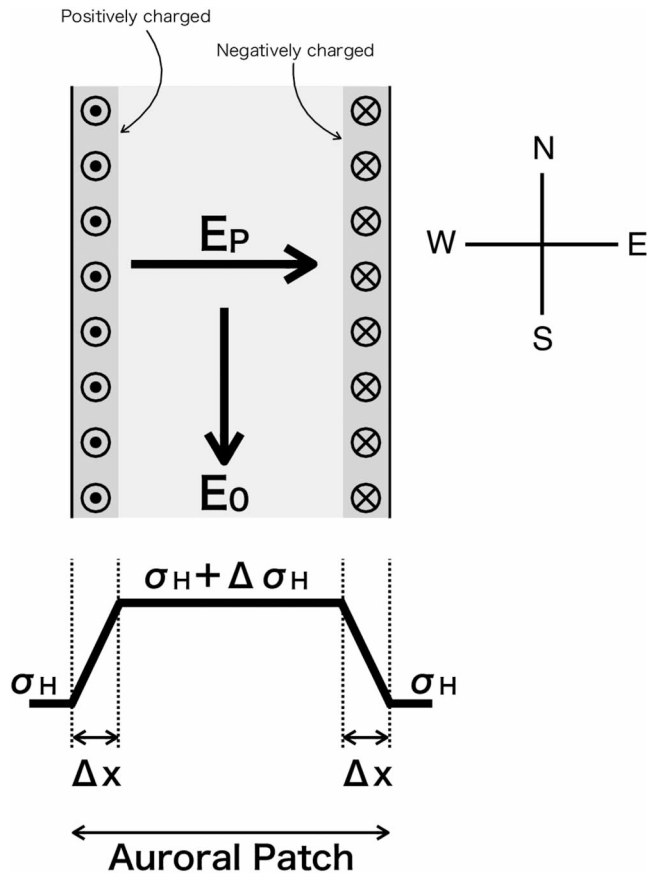


**Figure 9.** Conceptual diagram of the auroral patch elongated in the direction of the convective electric field (top) and the assumed the Hall conductance distribution (bottom).  $\Delta x$  is the width of the edge of the auroral patch shown by the dark gray shade. The upward and downward field-aligned currents are connected to the west (left) and east (right) side edge of the auroral patch, respectively.

experiment were likely to observed  $E_{PE}$  inside of the auroral patches “a,” “e,” and “f.”

### 5.5. Contribution of FACs to the Weakening of the Polarization Electric Field

Ground-based and satellite observations suggested that auroral patches were likely to appear with an FAC (Arnoldy et al., 1982; Fujii et al., 1985; Samara et al., 2015), and thus, FACs were considered as a possible cause of  $E_P$  weakening. When equation (1) was derived, the electric current divergence was assumed to be zero, indicating that the FAC was zero. If a FAC existed, equation (1) should be rewritten as

$$\nabla \cdot \{ \Delta \sigma_H (\mathbf{E}_0 \times \mathbf{e}_B) - \sigma_P \mathbf{E}_P \} = j_{\parallel} \quad (6)$$

where  $j_{\parallel}$  represents the FAC and  $\mathbf{e}_B$  is a unit vector along the magnetic field of the Earth. Fujii et al. (1985) and Gillies et al. (2015) suggested that the edges of auroral patches connect to FACs, therefore the widths of auroral patch edges shown in gray in Figure 9 were considered in our study. If  $\Delta x$  is defined as the horizontal width of the edge in the east-westward direction, equation (6) can be solved as follows:

$$\frac{\Delta \sigma_H}{\Delta x} E_0 - \sigma_P \frac{E_P}{\Delta x} = j_{\parallel}. \quad (7)$$

Since the eastward drift speed of the auroral patch was approximately 350 km/s, the east-west width of the auroral patch, nearly perpendicular to the convective electric field, was approximately 30 km.  $\Delta x$  was thus approximately estimated to 5–10 km. If the  $\Delta x$ ,  $E_0$ , and  $\Delta \sigma_H$  values shown in Tables 1 and 2 and a 40% weakened  $E_P$  are substituted into equation (6), the FAC can be estimated as 5.3–10.6, 6.2–12.8, 6.1–12.2, 7.8–15.6, and 8.3–16.7  $\mu\text{A}/\text{m}^2$  for auroral patches “a,” “b,” “c,” “e,” and “f.” In this situation, the downward and upward FACs were connected to the east and west side of the auroral patch edge, respectively. The Swarm satellite observation found a FAC of approximately 1  $\mu\text{A}/\text{m}^2$  inside the PsA patch at approximately 460-km altitude (Ling et al., 2017). Gillies et al. (2015) showed that a downward FAC of approximately 1–6  $\mu\text{A}/\text{m}^2$  can be seen

in the poleward boundary of a PsA patch recorded by the Swarm satellite observation performed during 2014. They also observed an upward FAC of approximately 1–2  $\mu\text{A}/\text{m}^2$  throughout the interior of the patch. Since they evaluated the relationship between the PsA which showed the patch structure and the FAC at the satellite altitudes (460–510 km), their results are comparable with our study. The FAC estimated in our study seemed to be 10 times larger than their observed results at a maximum. However,  $\Delta x$  could not be determined in detail because of the temporal resolution of the VHF radar and the FAC seemed to be mostly close to the Hall and Pedersen currents below the satellite altitude (Yokoyama & Stolle, 2017). Therefore, a FAC of approximately 5–10  $\mu\text{A}/\text{m}^2$  on the edge of the auroral patch in the dynamo region could have weakened  $E_P$ .

## 6. Conclusions

On 9 November 2015, the EISCAT UHF, VHF, Kiruna, Sodankylä radars, and KAIRA were simultaneously operated from 00:00 to 04:00 UT. During this night, the geomagnetic activity was elevated. Around 23:20 UT, the auroral breakup occurred. After that, the PsA appeared above Tromsø from 02:00 to 02:25 UT. The eastward drifting auroral patches in this interval were captured by the AWI and passed through the FOV of the UHF and VHF radars from 02:40 to 03:10 UT. Our study was primarily concerned with the motion of the auroral patches and the polarization electric fields generated inside auroral patches.

Based on AWI data, the drift speed of the auroral patches was estimated to range between 313 ( $\pm 83$ ) and 383 ( $\pm 101$ ) m/s and with an approximately eastward direction, corresponding to a southward electric field of 14.1 ( $\pm 3.7$ )–17.2 ( $\pm 4.5$ ) mV/m. The convective electric field in the ionosphere was derived by the EISCAT radars and KAIRA experiment to be approximately 14.6 mV/m in the southward direction. The electric

field estimated from the drift speed of the auroral patches approximately corresponded with the convective electric field, indicating that the motion of these auroral patches was probably governed by the convective electric field. Our results also suggest that the spatial distribution of the auroral patches reflects the distribution of cold plasma in the magnetosphere. Numerous previous, which also investigated auroral patches moving with ionospheric convection, studies exist, but those studies were carried out with instruments that have no height information such as all-sky imagers and the SuperDARN radar. Our study revealed the behavior of the patch motion with the height information.

The electron density at 80–120 km was enhanced by a factor of 2–4 inside the auroral patches. Further, the height-integrated Hall conductance was enhanced inside the auroral patches; however, there were no remarkable enhancements in the Pedersen conductance. Since the polarization electric field relative to the  $\Delta\sigma_H/\sigma_P$  was likely generated inside the auroral patches in this case, the polarization electric field was calculated based on current continuity. Enhanced ion velocities due to the polarization electric field was observed by the VHF at the dynamo region and was seen up to 200-km altitude; however, the absolute value of the ion velocity was approximately 40% of the expected value.

A FAC was suspected to contribute to the weakening of the polarization electric field. If a downward and upward FAC of roughly 5–10  $\mu\text{A}/\text{m}$  existed on the east and west edges of the auroral patches, respectively, the enhanced ion velocities could be explained by the polarization electric field. Although this FAC estimation was larger than observed by the SWARM satellites, the FAC existing on the edges of the auroral patches seems to have played a role in weakening the polarization electric field. The following conclusions were drawn.

The polarization electric fields perpendicular to the convective electric fields were generated inside the auroral patches due to Hall conductance enhancement. The upward and downward FACs contacting the west and east side edges of the auroral patches weakened the polarization electric field, which were of a magnitude slightly smaller than the convective electric field. The polarization electric field seemed to propagate upward from the dynamo region to at least 200-km altitude because the enhanced ion velocities was observed up to that altitude.

#### Acknowledgments

The production of this paper was supported by National Institute of Polar Research (NIPR) publication subsidy. T. Takahashi wishes to thank Y. Tanaka for the valuable comments and suggestions. I. Virtanen is funded by the Academy of Finland, application 285474. This work was carried out by the joint research program of the Institute for Space-Earth Environmental Research, Nagoya University. We are indebted to the director and staff of EISCAT for operating the facility and supplying the data. EISCAT is an international association supported by research organizations in China (CRIRP), Finland (SA), Japan (NIPR and ISEE), Norway (NFR), Sweden (VR), and the United Kingdom (NERC). The ground optical data used in this paper can be provided by NIPR (<http://pc115.seg20.nipr.ac.jp/www/opt/>).

#### References

- Akasofu, S. I., Meng, C. I., & Kimball, D. S. (1966). Dynamics of the aurora—VI: Formation of patches and their eastward motion. *Journal of Atmospheric and Terrestrial Physics*, 28, 505–511.
- Amm, O., Fujii, R., Vanhamäki, H., Yoshikawa, A., & Ieda, A. (2013). General solution for calculating polarization electric fields in the auroral ionosphere and application examples. *Journal of Geophysical Research: Space Physics*, 118, 2428–2437. <https://doi.org/10.1002/jgra.50254>
- Arnoldy, R. L., Dragoon, K., Cahill, J. L. J., Mende, S. B., & Rosenberg, T. J. (1982). Detailed correlations of magnetic field and riometer observations at  $L=4.2$  with pulsating aurora. *Journal of Geophysical Research*, 87, 10,449–10,456.
- Billitz, D. (2001). International reference ionosphere 2000. *Radio Science*, 36, 261–275.
- Brekke, A. (Ed.) (1997). *Physics of the upper polar atmosphere* Edited by Brekke, A. New York: John Wiley.
- Davis, T. N. (1978). Observed characteristics of auroral forms. *Space Science Reviews*, 22, 77–113.
- de la Beaujardiere, O., Vondrak, R., & Baron, M. (1977). Radar observations of electric fields and currents associated with auroral arcs. *Journal of Geophysical Research*, 82(32), 5051–5062. <https://doi.org/10.1029/JA082i032p05051>
- Fujii, R., Oguti, T., & Yamamoto, T. (1985). Relationships between pulsating auroras and field-aligned currents. *Memoirs of National Institute of Polar Research*, 36, 95–103.
- Gillies, D. M., Knudsen, D., Spanswick, E., Donovan, E., Burchill, J., & Patrick, M. (2015). Swarm observations of field-aligned currents associated with pulsating auroral patches. *Journal of Geophysical Research: Space Physics*, 120, 9484–9499. <https://doi.org/10.1002/2015JA021416>
- Haerendel, G. (2007). Auroral arcs as sites of magnetic stress release. *Journal of Geophysical Research*, 112, A09214. <https://doi.org/10.1029/2007JA012378>
- Hosokawa, K., Kadokura, A., Sato, N., Milan, S. E., Lester, M., Björnsson, G., & Saemundsson, T. (2008). Electric field modulation behind pulsating aurora. *Journal of Geophysical Research*, 113, A11322. <https://doi.org/10.1029/2008JA013601>
- Hosokawa, K., Ogawa, Y., Kadokura, A., Miyaoka, H., & Sato, N. (2010). Modulation of ionospheric conductance and electric field associated with pulsating aurora. *Journal of Geophysical Research*, 115, A03201. <https://doi.org/10.1029/2009JA014683>
- Ishii, M., Oyama, S., Nozawa, S., Fujii, R., Sagawa, E., Watari, S., & Shinagawa, H. (1999). Dynamics of neutral wind in the polar region observed with two Fabry-perot interferometers. *Earth Planets Space*, 51, 833–844.
- Kurihara, J., Oyama, S., Nozawa, S., Tsuda, T. T., Fujii, R., Ogawa, Y., et al. (2009). Temperature enhancements and vertical winds in the lower thermosphere associated with auroral heating during the delta campaign. *Journal of Geophysical Research*, 114, A12306. <https://doi.org/10.1029/2009JA014392>
- Ling, J., Yang, B., Donovan, E., Burchill, J., & Knudsen, D. (2017). Ionospheric electron heating associated with pulsating auroras: A swarm survey and model simulation. *Journal of Geophysical Research: Space Physics*, 122, 8781–8807. <https://doi.org/10.1002/2017JA024127>
- Marklund, G. (1984). Auroral arc classification scheme based on the observed arc-associated electric field pattern. *Planetary and Space Science*, 32, 193–211.

- McKay-Bukowski, D., Vierinen, J., Virtanen, I. I., Fallows, R., Postila, M., Ulich, T., et al. (2015). KAIRA: The Kilpisjärvi Atmospheric Imaging Receiver Array—System overview and first results. *Transactions on Geoscience and Remote Sensing*, 53(3), 1440–1451. <https://doi.org/10.1109/TGRS.2014.2342252>
- Miyoshi, Y., Oyama, S., Saito, S., Kurita, S., Fujiwara, H., Kataoka, R., et al. (2015). Energetic electron precipitation associated with pulsating aurora: EISCAT and Van Allen Probe observations. *Journal of Geophysical Research: Space Physics*, 120, 2754–2766. <https://doi.org/10.1002/2014JA020690>
- Mozer, F. S. (1970). Electric field mapping in the ionosphere at the equatorial plane. *Planetary and Space Science*, 18, 259–263.
- Oguti, T. (1976). Recurrent auroral patterns. *Journal of Geophysical Research*, 81, 1782–1786. <https://doi.org/10.10291041/JA081i010p01782>
- Picone, J. M., Hedin, A. E., & Drob, D. P. (2002). NRLMSISE-00 empirical model of the atmosphere: Statistical comparisons and scientific issues. *Journal of Geophysical Research*, 107(A12), 1468. <https://doi.org/10.1029/2002JA009430>
- Rishbeth, H., & Williams, P. J. S. (1985). The EISCAT ionospheric radar: The system and its early results. *Quarterly Journal of the Royal Astronomical Society*, 26, 468–512.
- Samara, M., Michell, R. G., & Redmon, R. J. (2015). Low-altitude satellite measurements of pulsating auroral electrons. *Journal of Geophysical Research: Space Physics*, 120, 8111–8124. <https://doi.org/10.1002/2015JA021292>
- Thébault, E., Finlay, C. C., Beggan, C. D., Alken, P., Aubert, J., Barrois, O., et al. (2015). International geomagnetic reference field: The 12th generation. *Earth, Planets and Space*, 67, 79. <https://doi.org/10.1186/s40623-015-0228-9>
- Vallinkoski, M. (1988). Statistics of incoherent scatter multiparameter fits. *Journal of Atmospheric and Terrestrial Physics*, 50, 839–851.
- Virtanen, I. I., McKay-Bukowski, D., Vierinen, J., Aikio, A., Fallows, R., & Roininen, L. (2014). Plasma parameter estimation from multi-static, multibeam incoherent scatter data. *Journal of Geophysical Research: Space Physics*, 119, 10,528–10,543. <https://doi.org/10.1002/2014JA020540>
- Yang, B., Donovan, E., Liang, J., Ruohoniemi, J. M., & Spanswick, E. (2015). Using patchy pulsating aurora to remote sense magnetospheric convection. *Geophysical Research Letters*, 42, 5083–5089. <https://doi.org/10.1002/2015GL064700>
- Yokoyama, T., & Stolle, C. (2017). Low and midlatitude ionospheric plasma density irregularities and their effects on geomagnetic field. *Space Science Reviews*, 206, 495–519. <https://doi.org/10.1007/s11214-016-0295-7>

## Erratum

In the originally published version of this article, the equation number (4) was left out of the phrase “equation (4)” in four instances in Section 5.4. The text has been updated, and the present version may be considered the authoritative version of record.